Article

J. Mex. Chem. Soc. **2012**, *56(3),* 346-350

ISSN 1870-249X

Elucidating the Catalytic Role of Mg(II) in the Intramolecular Proton Transfer Reaction in Thymine

Stefan Vogt-Geisse, Soledad Gutiérrez-Oliva, Bárbara Herrera, and Alejandro Toro-Labbé*

Laboratorio de Química Teórica Computacional (QTC), Facultad de Química, Pontificia Universidad Católica de Chile, Vicuña Mackenna 4860, Macul. Santiago, Chile. atola@puc.cl

Received December 01, 2011; accepted May 23, 2012

Abstract. In the framework of the reaction force analysis a study of the mechanism of the 1-3 intramolecular proton transfer in free and Mg (II) coordinated Thymine was done in terms of the reaction electronic flux and Wiberg bond orders. Profiles of these properties evidentiated differences between the proton transfer mechanisms induced by the presence of Mg(II) cation. A significative lowering in the activation energy put forward the catalytic effect of Mg. The reaction force analysis allows a precise identification of the catalytic effect thus uncovering the physical nature of activation energies. While in the free Thymine electronic polarization and transfer processes are present separately, in the Mg(II) coordinated Thymine both effects are observed simultaneously and are localized on the ring in the molecular topology. It is argued that the difference in the charge transfer mechanism leads to a more stable enol form in the Mg(II) coordinated Thymine.
Keywords: Reaction Force, Reaction Electronic Flux, Proton Transfer Reaction, Thymine.

Resumen. En el marco del análisis basado en la Fuerza de la reacción, estudiamos el mecanismo de la transferencia protónica en timina y en timina coordinada con Mg(II) mediante el uso del Flujo Electrónico de Reacción en combinación con los ordenes de enlace de Wiberg. Los perfiles de estas propiedades muestran interesantes diferencias entre las dos reacciones de transferencia protónica y se observa una disminución significativa de la barrera energética estableciéndose el efecto catalítico del catión Mg(II). El análisis basado en la Fuerza de la Reacción permitió además establecer la naturaleza física de las barreras energéticas. También se observó que en Timina libre los efectos de polarización y transferencia electrónica ocurren separadamente mientras que en el complejo con magnesio estos efectos ocurren de manera simultánea.
Palabras clave: Fuerza de reacción, flujo electrónico de reacción, reacciones de transferencia protónica, timina.

Introduction

The interaction between biomolecules and metal cations has been of high interest in recent decades due to the regulating properties within a living organisms which these cations are attributed to have [1-3]. Magnesium is especially interesting in this context, since it can form very stable complexes with many ligands of different nature. In particular Russo et al have shown that Mg2+ has special affinity for DNA and RNA nucleobases [4] where it can play an important role in the stabilization of secondary and tertiary structures [5, 6]. In this work we revisit the 1,3 intramolecular proton transfer in the DNA base thymine and analyze the role of the Mg (II) cation in the reaction mechanism. This tautomeric process transforms the keto form into its less common enol counterpart (Figure 1). The Mg-thymine tautomer chosen for this study is one of the most stable forms [4] where the 1,3 proton transfer reaction take place, other Mg-thymine tautomers do not present the reaction. On the other hand, it should be mentioned that the 1,3 proton transfer tautomerization reaction is quite important in biochemistry since it is considered as a possible molecular mechanism that may produce spontaneous mutations and activation of cancer processes [7, 8].

The scope of this paper is on elucidating the 1,3 proton transfer reaction mechanism through the use of the reaction electronic flux (REF) and local electronic properties like bond orders and population analysis to identify and rationalize polarization and transfer effects that drives the reactions. To find out the differences induced by the Magnesium cation in the charge transfer mechanism a thorough analysis of the named properties within the framework of the reaction force is made.

Theoretical Background

Reaction Force Profiles

The Reaction Force is defined as the negative derivative of the energy with respect to the reaction coordinate [9-11]

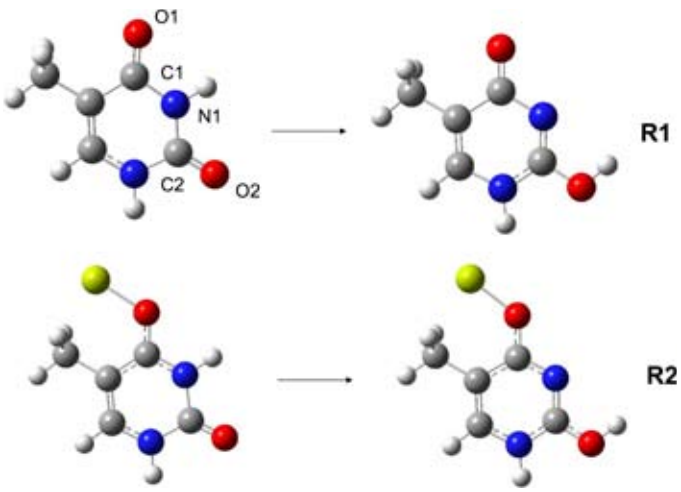

Fig. 1. Sketch of the proton transfer reactions R1 and R2.

$$F(\xi) = -\frac{dE}{d\xi} \quad (1)$$

For a chemical reaction where reactants and products are separated by an energy barrier, F(ξ) presents two critical points which are a minimum at ξ_1 and a maximum at ξ_2. These points define regions along ξ in which different kind of processes might be taking place. The reactant region ($\xi_R \leq \xi \leq \xi_1$) is where reactants are getting ready for reaction, here mainly structural reordering takes place. The transition state region ($\xi_1 < \xi < \xi_2$) is characterized by a marked electronic reordering, while in the product region ($\xi_2 \leq \xi \leq \xi_P$) structural relaxation is predominant [9-12].

The energy involved as the reaction advances along the reaction coordinate can be characterized through the works determined at the different steps of the reaction:

$$W_1 = -\int_{\xi_R}^{\xi_1} F(\xi)d\xi > 0; \quad W_2 = -\int_{\xi_1}^{\xi_0} F(\xi)d\xi > 0;$$
$$W_3 = -\int_{\xi_0}^{\xi_2} F(\xi)d\xi < 0; \quad W_4 = -\int_{\xi_2}^{\xi_P} F(\xi)d\xi < 0 \quad (2)$$

with ξ_0 the position of the transition state. The activation energy ($\Delta E^{\neq}$) can be therefore rationally partitioned as [11, 13-17]:

$$\Delta E^{\neq} = W_1 + W_2. \quad (3)$$

An important result that comes out from the partition given by Equation (3) is that the physical nature of $\Delta E^{\neq}$ can now be attributed through the relative weight of the components W1 and W2 [16, 17]. Similarly the reaction force provides a framework for a rational partition of the reaction energy:

$$\Delta E^{\circ} = W_1 + W_2 + W_3 + W_4 \quad (4)$$

Reaction Electronic Flux

The chemical potential is an important global property within conceptual DFT and is defined as [18, 19]:

$$\mu = \left(\frac{\partial E}{\partial N}\right)_{v(\mathbf{r})} \quad (5)$$

it represents the escaping tendency of the electronic cloud from an equilibrium position. A working expression for μ can be obtained through finite difference aproximation:

$$\mu \cong -\frac{1}{2}(I + A) \quad (6)$$

which can be further simplified through Koopmans' theorem [20] involving the energy of the highest occupied and lower unoccupied molecular orbitals ε_H and ε_L, respectively:

$$\mu \cong -\frac{1}{2}(\varepsilon_L + \varepsilon_H) \quad (7)$$

To gain detailed insights into the electron transfer mechanism present in a reaction a new useful descriptor, which arises from the chemical potential taken along a reaction coordinate, has been introduced: the Reaction Electronic Flux [12, 21-23]. It is defined as the negative derivative of the chemical potential with respect to the reaction coordinate:

$$J(\xi) = -\left(\frac{d\mu}{d\xi}\right) \quad (8)$$

With the help of this descriptor it is possible to clearly identify where, along the reaction coordinate, electronic changes are happening in a chemical reaction. Furthermore following the thermodynamic analogy, regions with J (ξ) > 0 are associated with spontaneous arrangements of the electronic density driven by bond strengthening/forming processes whereas J (ξ) < 0 should be associated to non-spontaneous change of the electron density driven by bond weakening/breaking processes [22-24]. In this context, the reaction electronic flux identifies and rationalizes the electronic activity taking place along the reaction coordinate, in doing so, it gives a very neat and complete characterization of the mechanism of chemical reactions [12, 22-24].

Computational Details

All calculations were carried out at the density functional theory (DFT) level, using the hybrid B3LYP functional and the 6-311++G(d,p) basis set [25], with the GAUSSIAN 03 package [26]. Transition states were located using the quadratic synchronous transit (QST2) approach [27] and frequency calculations were performed in order to check the stationary states. The profiles of energy and reaction force were obtained through the intrinsic reaction coordinate (IRC=ξ) procedure, which is arbitrarily zero at the transition state position [28]. The profiles of energy, reaction force, chemical potential and reaction electronic flux were obtained through single point calculations on the previously optimized geometries obtained from the IRC procedure. The chemical potential along the reaction coordinate was determined through Eqn.(7) using HOMO and LUMO orbital energies. Additionally the profiles were checked with ionization potential and electron affinities for the total chemical potentials (Eqn. (6)), obtaining an excellent agreement. Since in this work the reaction electronic flux is analyzed along a reaction coordinate, it appears that relative values of it are used to describe the electronic activity during the reactions. In this context the error of using the Koopmans' theorem to determine the chemical potential and the REF from DFT orbital energies will not play a role in the present analysis. More details on the use of Koopmans' theorem in DFT calculations can be found elsewhere [29]. Natural Bond Orbital (NBO) [30] analysis was carried out in which the Wiberg bond orders were obtained along the reaction coordinate to explain in more detail the electronic activity taking place during the reactions.

Results and Discussion

Energy and Reaction Force Profiles

Figure 1 sketches the ketoenol tautomerization in free (R1) and Mg(II) coordinated thymine (R2) in which a proton from N1 is transferred to O2. The scope of this work is on the 1-3 intramolecular proton transfer reaction in which the main electronic changes occur. In R2 we are mostly interested in characterizing the catalytic effect of the cation as an expectator of the proton transfer process. The second step of the reaction, in which the cation participates actively and produces a bicoordinated product, has been the focus of previous studies [16, 31]. Various gas phase [Mg· · ·Nucleobase] complexes have been produced experimentally through photo-induced reactions by using the laser ablation combined with the supersonic expansion technique, using this setting, intramolecular proton transfer has been detected [32]. Figure 2 shows the energy profiles and reaction force profiles for reactions R1 and R2.

Due to the presence of the magnesium cation the reaction goes from being significantly endoenergetic (19.1 kcal/mol) to being nearly isoenergetic with a reaction energy of 0.45 kcal/mol. An important result of this reaction becomes clear when analyzing the reaction barriers since a decrease in 5 kcal/mol is observed in R2, this catalytic effect should be associated to the presence of Mg(II) [16]. Furthermore, comparing the reaction works associated to the elementary steps of these reactions it can be noticed that the shrinkage of the barrier in the forward reaction is exclusively due to a diminution of W_1, indicating that Magnesium affects the barrier mainly in the reactant region, see Table 1. The B3LYP functional generally leads to acceptable energy barriers, although there are cases in which they are underestimated. However this should not change the relative weight of the components $\{W_1, W_2, W_3, W_4\}$ in the forward and reverse barriers.

Reaction Electronic Flux (REF)

Figure 3 shows the profile of reaction electronic flux for R1 and R2. A slight increase of the REF in the reactant region is observed in R1 thus indicating that the reaction initiates with some electronic activity that is driven by bond strengthening/forming processes. In this context, in R1 the reaction work W_1 should be associated to a combination between structural and electronic effects. In contrast to this, in R2 a zero flux regime spans over the entire reactant region, indicating that there is no electronic activity other than the basal one and then W_1 should be safety associated to structural reorderings that prepare the reaction to the forthcoming electronic activity that shows up within the transition state region. This is an important result since the physical nature of the activation energies and its components becomes aparent. Entering the TS region opposite trends of REF are observed in the two reactions, in R1 an intense negative peak is observed indicating that bond weakening/breaking processes are driving the electronic activity; in R2 a slight positive increase can be appreciated thus indicating that electronic activity is driven by bond strengthening/forming processes. The reaction force analysis indicates that the reaction work W_2 is mainly due to electronic activity, further light on the characterization of the physical nature of activation energies comes from the REF analysis. First we note that the values of W_2 in R1 and R2 are quite similar, but the REF

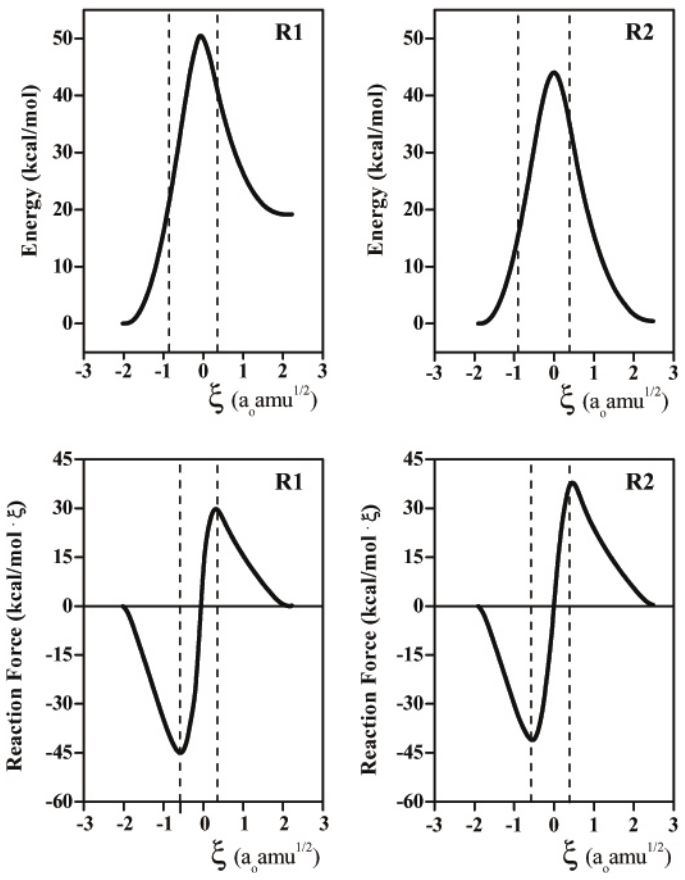

Fig. 2. Relative energy (in kcal/mol) and reaction force (in kcal/mol·ξ) profiles of the proton transfer reactions R1 and R2.

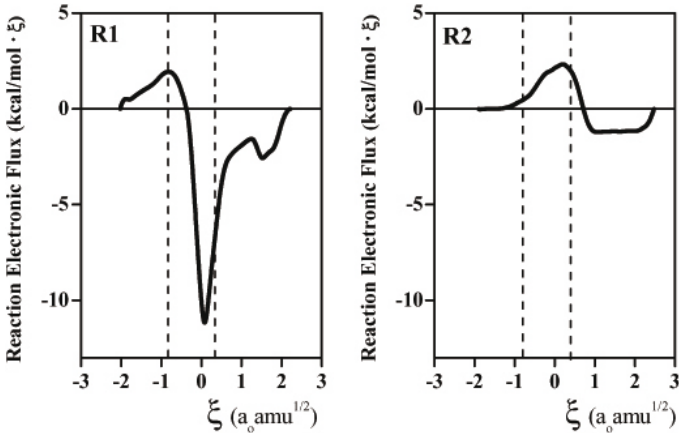

Fig. 3. Reaction electronic flux profiles (in kcal/mol·ξ) for R1 and R2.

Table 1: Reaction energy ($\Delta E°$), forward and reverse activation energies $\{\Delta E^{\neq}_{f}, \Delta E^{\neq}_{r}\}$; reaction works and their relative weights in the activation barriers. All values are in kcal/mol.

Reaction	$\Delta E°$	$\Delta E^{\neq}_{f}$	$\Delta E^{\neq}_{r}$	W_1	W_2	$-W_3$	$-W_4$
R1	19.10	49.61	30.51	32.64 (66%)	16.97 (34%)	7.00 (23%)	23.51 (77%)
R2	0.45	44.21	43.76	27.11 (61%)	17.10 (39%)	9.37 (21%)	34.39 (79%)

behavior indicate that they come from opposite processes: in R1 the non-spontaneous bond weakening/breaking processes determine W_2 whereas in R2 this reaction work is determined by spontaneous bond strengthening/forming processes. This is crucial information in the characterization of the physical nature of activation energies. Finally, in the product region R1 and R2 present negative flux which fades out towards a zero flux regime at the products of the reactions.

Bond Order Analysis

It has been shown through the REF analysis that the Mg cation induces a different mechanism for the proton transfer process. Further insights will give the Wiberg bond order [30]. Figure 4 displays the bond orders of the relevant bonds in both reactions. First we observe that the presence of the Mg cation weakens the C1O1 bond and strengthens the C1N1 bond. The same effect but with less intensity is observed within the N1C2 and C2O2 bond orders where the former is slightly weakened and the latter is strengthened. Complementing this information, the natural charges indicate that O1 gains charge while N1 and O2 loose charge. This suggests that there is a charge migration towards the Mg cation, which affects most the atoms and bonds close to it.

On the other hand, it can be observed that in both reactions the most significant changes of all bond orders occur at the TS region confirming that in this region most electronic activity is concentrated. In R1 the strengthening of the C1O1 and N1C2 bonds explain the spontaneous electronic reordering observed within the reactant region whereas the weakening of C1O1 and C2O2 explain the negative peak observed in the REF profile in terms of non-spontaneous electronic activity. In R2 the electronic activity observed in the REF profile is driven by the strengthening of the C1O1 and N1C2 bonds.

Entering the product region of R2 a point of high electronic delocalization is observed where three bond orders take the same value (C1N1, N1C2 and C2O2). On the other hand in R1 only the N1C2 and C2O2 bond orders cross at the transition state region. So, the product region is characterized by a high delocalization in R2 as all bond orders remain close by, since the new N1C2 double bond is delocalized over the ring system. In R1, on the other hand, the delocalization in the product region is quite the same as in the reactant region. It seems that the high delocalization in the product region induced by the presence of Mg(II) cation stabilizes the enol form in R2.

In the light of the above results, reaction mechanisms can be foreseen. In R1 polarization is necessary to break the electronic delocalization in the ring system, evidenciated by the close values of the bond orders C1N1 and N1C2, in order to activate the proton transfer. On the other hand, in R2, the positive charge of the Mg cation polarizes the electronic density activating the ring system and making a large polarization flux needless. This is the main effect that makes Mg(II) be a good catalyst of the proton transfer reaction. It is important to stress the fact that the difference in the proton transfer mechanism induced by Mg has no effect on the W_2 component of the energy barrier but, as already mentioned, it changes its physical nature and provides a way to reach a more delocalized and hence more stable enol form.

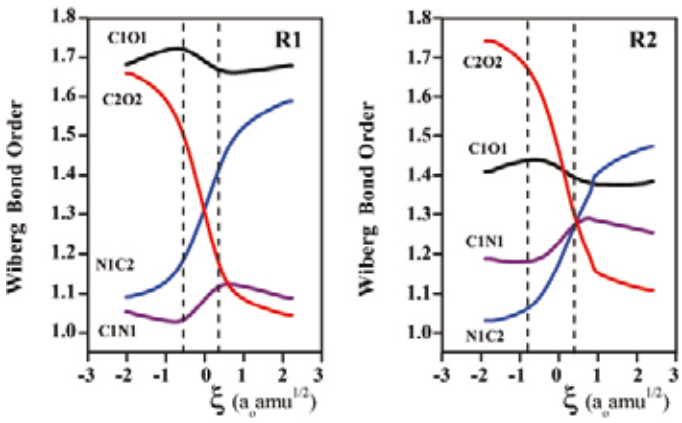

Fig. 4. Wiberg bond order on the reactive bonds of R1 and R2.

Concluding Remarks

In this study, dedicated to our friend José Luis Gazquez, an important catalytic effect of the Mg(II) cation on the intramolecular proton transfer reactions in thymine was observed, and the physical nature of the activation energies was elucidated. In naked thymine structural and electronic effects define the activation energy whereas in the Mg-assisted reaction both effects were neatly separated and take place within different reaction regions.

The reaction electronic flux evidenciated important differences in the proton transfer mechanisms, in R1 the reaction is activated through spontaneous electronic activity taking place at the reactant region strengthening specific bonds whereas R2 is activated through structural reordering that facilitates the forthcoming electronic activity. The presence of the Mg(II) cation prevents the need of an initial polarization to activate the proton transfer. The electronic delocalization pattern was clearly identified and the Mg(II) effect on the charge density through the whole reaction coordinate was shown.

Acknowledgments

This manuscript is dedicated to Professor José Luis Gázquez, a brilliant scientist and a very good friend. We would like to take this opportunity to thank José Luis for his enlightening and pionnering works on conceptual DFT. Financial support from FONDECYT through projects N° 1090460, N° 1120093 and N° 1100881 is acknowledged.

References

1. Hud, N. V.; Polak, M. *Curr. Opin. Struct. Biol.* **2001**, *11*, 293.
2. Sclavi, B.; Sullivan, M.; Chance, M.; Bernowitz, M.; Woodson, S. *Science*, **1998**, *279*, 1940.
3. Anastassopoulou, J. *J. Mol. Struct.* **2003**, *19*, 651.
4. Russo, N.; Toscano, M.; Grand, A. *J. Phys. Chem. A* **2003**, *107*, 11533.
5. Anastassopoulou, J.; Theophanides, T. *Crit. Rev. Oncol. Hematol.* **2002**, *42*, 79.
6. Tajmir-Riahi, H. A.; Theophanides, T. *Inorg. Chim. Acta* **1983**, *80*, 223.
7. Podolyan, Y.; Gorb, L.; Leszczynski, *J. Int. J. Mol. Sci.* **2003**, *4*, 410.
8. Danilov, V. I.; Anisimov, V. M.; Kurita, N.; Hovorun, D. *Chem. Phys. Lett.* **2005**, *412*, 285.
9. Toro-Labbé, A. *J. Phys. Chem. A* **1999**, *103*, 4398-4403.
10. Politzer, P.; Toro-Labbé, A.; Gutiérrez-Oliva, S.; Herrera, B.; Jaque, P.; Concha, M.; Murray, J. *J. Chem. Sci.* **2005**, *117*, 467-472.
11. Toro-Labbé, A.; Gutiérrez-Oliva, S.; Concha, M.; Murray, J.; Politzer, P. J. *Chem. Phys.* **2004**, *121*, 4570-4576.
12. Vogt-Geisse, S.; Toro-Labbé, A. *J. Chem. Phys.* **2009**, *130*, 244308.
13. Gutiérrez-Oliva, S.; Herrera, B.; Toro-Labbé, H.; Chermette, A. *J. Phys. Chem. A* **2005**, *109*, 1748-1751.
14. Herrera, B.; and Toro-Labbé, A. J. Chem. Phys., **2004**, *121*, 7096-7102.
15. Martínez, J.; Toro-Labbé, A. *Chem. Phys. Lett.* **2004**, *392*, 132-139.
16. Rincón, E.; Jaque, P.; Toro-Labbé, A. *J. Phys. Chem.* **2006**, *110*, 9478.
17. Burda, J. V.; Toro-Labbé, A.; Gutiérrez-Oliva, S.; Murray, J. S.; Politzer, P. *J. Phys. Chem.* **2007**, *111*, 2455.
18. Parr, R.; Yang, W. *Density Functional Theory of Atoms and Molecules*. Oxford University Press, New York **1989**.
19. Geerlings, P.; De Proft, F.; Langenaeker, W. Chem. Rev., **2003**, *103*, 1793-1873.
20. Koopman, T. A. Physica, **1933**, *1*, 104.
21. Flores, P.; Gutiérrez-Oliva, S.; Silva, E.; Toro-Labbé, A. *J. Mol. Struct.* (Theochem), **2010**, *943*, 121-126.
22. Echegaray, E.; Toro-Labbé, A. *J. Phys. Chem. A* **2008**, *112*, 11801.
23. Cerón, M. L.; Echegaray, E.; Gutiérrez-Oliva, S.; Herrera, B.; Toro-Labbé, A. Science China: *Chemistry*, **2011**, *54*, 1982-1988.
24. Duarte, F.; Toro-Labbé, A. *J. Phys. Chem. A* **2011**, *115*, 3050.
25. Becke, A. D. *J. Chem. Phys.* **1993**, *98*, 5648-5652.
26. Frisch, M. J. *et al.* Gaussian Inc., Pittsburgh, PA **2003**.
27. Peng, C.; Ayala, P. Y.; Schlegel, H. B.; Frisch, M. J. J. *Comp. Chem.* **1996**, *17*, 49.
28. Fukui, K. *Acc. Chem. Res.* **1981**, *14*, 363.
29. Tsuneda, T.; Song, J. W.; Suzuki, S.; Hirao, K. *J. Chem. Phys.* **2010**, *133*, 174101.
30. Reed, A.; Curtiss, L. A.; Weinhold, F. *Chem. Rev.* **1988**, *88*, 899.
31. Rincón, E.; Toro-Labbé, A. *Chem. Phys. Lett.* **2007**, *438*, 93.
32. Sun, J. L.; Liu, H.; Wang, H. M.; Han, K. L.; Yang, S. *Chem. Phys. Lett.* **2004**, *392*, 285.